INTERNATIONAL JOURNAL OF HYDROGEN ENERGY 45 (2020) 20776–20786

Available online at www.sciencedirect.com

ScienceDirect

journal homepage: www.elsevier.com/locate/he

Sputter-etching treatment of proton-exchange membranes: Completely dry thin-film approach to low-loading catalyst-coated membranes for water electrolysis

Tomáš Hrbek, Peter Kúš, Yurii Yakovlev, Jaroslava Nováková, Yevheniia Lobko, Ivan Khalakhan, Vladimír Matolín, Iva Matolínová*

Charles University, Faculty of Mathematics and Physics, Department of Surface and Plasma Science, V Holešovičkách 2, 180 00 Prague 8, Czech Republic

HIGHLIGHTS

- Surface of proton-exchange membrane was modified by dry sputter-etching process.
- Created fiber-like structure can serve as a catalyst support for PEM-WE applications.
- Level of porosity can be tuned by varying the working pressure during the treatment.
- CCM with modified PEM and thin-film catalysts was prepared solely by dry technique.
- High performance was achieved with the combined Pt + Ir loading of just 220 μg cm^{-2}.

GRAPHICAL ABSTRACT

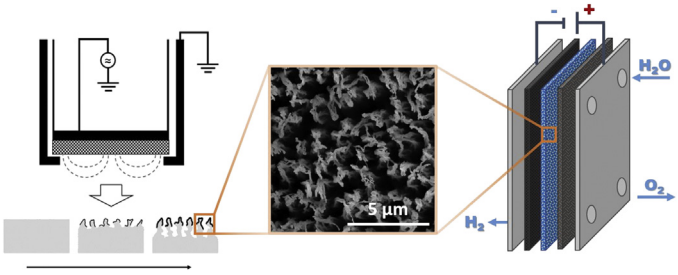

ARTICLE INFO

Article history:
Received 14 April 2020
Received in revised form
26 May 2020
Accepted 27 May 2020
Available online 25 June 2020

Keywords:
PEM water electrolysis
Magnetron sputtering

ABSTRACT

Simultaneous plasma etching of a proton-exchange membrane (PEM) and deposition of a cerium oxide layer during reactive magnetron sputtering leads to the formation of a pronounced fiber-like structure on its surface. The level of structural porosity can be adjusted by varying the working pressure during the process. A PEM treated this way can be subsequently coated with a thin layer of iridium, forming an anode-side catalyst-coated membrane (CCM) for applications in water electrolysis. Due to the significantly enlarged surface of the membrane, there is no necessity for any additional, potentially corroding, support nanoparticles to achieve efficient in-cell operation. Moreover, utilizing a rotatory frame-shaped substrate holder and a multitarget deposition apparatus, the sputter-etching process can be used in the preparation of a full anode/cathode thin-film CCM in a single

* *Corresponding author.*
E-mail address: peter.kus@mff.cuni.cz (P. Kúš).
https://doi.org/10.1016/j.ijhydene.2020.05.245

Membrane modification
Catalyst support
Thin-film catalyst

vacuum entry. This structure yields remarkable performance characteristics in an electrolyzer cell, considering its low combined noble metal loading of just 220 μg cm^{-2}. Using this completely dry process for CCM manufacturing may facilitate efficient large-scale future production.

Introduction

Nowadays, storing energy from renewable, yet intermittent, power sources (e.g. wind and solar) is gaining attention since it plays a pivotal role in the transition to a carbon emission-free society. In this regard, numerous electrical energy storage systems are being proposed, ranging from mechanical through thermal to electrochemical systems [1–4]. Due to the complex nature of energy generation, distribution and other associated specifications, it is nontrivial to evaluate which particular system is ideal for any given application. Nonetheless, it is reasonable to expect that the greater the universality and scalability of any particular technology, the better the chances of its widespread implementation across the electrical grid. The concept of a hydrogen economy therefore seems to be very attractive [5–8].

The hydrogen economy is built around the "power-to-gas" conversion of electricity into H_2 at times of energy overproduction, and its subsequent utilization in various ways. The very diversity with which hydrogen can eventually be utilized makes this an outstanding concept. Stored hydrogen does not necessarily have to be converted back to electricity on-site via fuel cells but can be either injected into the existing natural gas network, processed as an industrial commodity or be dispatched as a versatile energy vector. Regardless of which pathway is ultimately chosen, the key inseparable technology necessary for a functioning hydrogen economy is water electrolysis; i.e. the electrochemical splitting of water into gaseous hydrogen and oxygen [9,10].

Among many different types of water electrolyzers, those with a proton-exchange membrane (PEM-WE) are arguably the most suitable for industrial scale-up [11,12]. However, there are some technological challenges that need to be resolved before PEM-WEs can enter mass production. Most R&D efforts are dedicated to addressing the dependence on noble metals that are currently the only active and stable catalysts suitable for individual reactions; Ir for the oxygen evolution reaction (OER) on the anode [13,14] and Pt for the hydrogen evolution reaction (HER) on the cathode [15,16]. Although various multimetal oxides [17,18], complex alloys [19,20] or core-shell structures [21–23] within which the noble metal is substituted by more abundant elements are being investigated, the most common and reliable way to reduce Pt and Ir loading is by their thorough dispersion over supporting nanoparticles or other objects with a large surface-to-bulk ratio. On the cathode, Pt is typically carried on some sort of carbon-based material [24]; this method has been conveniently adapted from fuel cell technologies [25]. However, the situation is much more complicated on the anode of PEM-WE, where high operational potentials render carbon nanoparticles inappropriate [26,27]. To identify a material capable of withstanding up to 2 V while remaining sufficiently corrosion resistant and electrically conductive is a non-trivial problem. Some metal oxides [28–32] and carbides [33–37] have been reported, within certain limits, to substitute for carbon in its role as a catalyst support but the long-term stability of such materials is not always satisfactory.

In this report, we propose an innovative, yet straightforward and industrially adaptable approach to circumvent the principal drawback of PEM-WE technology, i.e. the problem of lowering the Ir loading on the anode side of the cell without a reliance on complex multi-elemental catalysts or non-carbon catalyst supports. The approach is based on utilizing magnetron sputtering. The novelty of our patented method is in the simultaneous plasma etching of a PEM and deposition of a CeO_x thin film onto its surface. The CeO_x layer serves as a masking element that prevents loss of material at sites with sufficient coverage. In contrast, unprotected sites are continually etched (see Fig. 1). This results in the formation of a fiber-like structure with cross-sectional dimensions much smaller than their height. The modified surface of the PEM itself is therefore sufficiently large to carry a subsequently deposited thin-film catalyst completely on its own. Additional information on the mechanism of sputter-etching and its effect on carbon-based materials can be found in our previous publications [38–42].

It was previously shown that magnetron sputtering is a viable method for preparing low-loading catalysts with remarkable specific performances for fuel cells and water electrolyzers [43–51]. However, to obtain maximal performance and due to the fact that sputtering forms compact thin layers, deposition had to be carried out onto a surface of nanoparticles with a high degree of porosity. The presence of a fiber-like structure made of the PEM itself significantly simplified this problem. It should be also pointed out, that a simple roughening of the PEM due to plasma etching was previously investigated and indeed led to a notable improvement in performance [52]. However, the absence of simultaneous material deposition, and hence the lack of a masking effect, meant that the roughness was much less than in our case. A very important factor that distinguishes our approach from other methods of growing anisotropic supports or catalysts, such as organic pigment nanowhiskers [53], nanowire structures [54], nanorod arrays [55], nanosheets [56] or nanotubes [57] is that no wet process is involved and no laminate transfer of material to the PEM is required; the procedure is completely dry. Clean pristine PEM is placed in a dual magnetron deposition system (one magnetron for the CeO_2

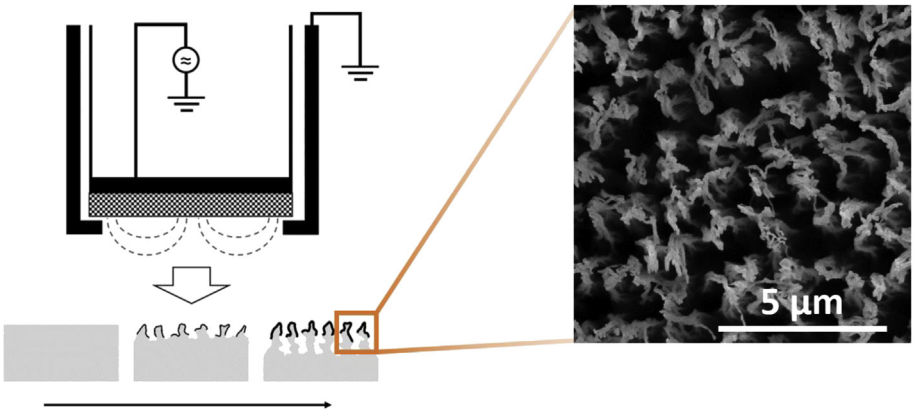

Fig. 1 – Schematic representation of sputter-etching of a PEM surface.

target, another for the catalyst target) and after individual sputterings, the modified sputter-etched catalyst-coated membrane (CCM) is ready for its use in a water electrolyzer as part of the membrane electrode assembly (MEA).

Recently we have shown that our membrane comprising a modified surface covered with a thin-film Pt catalyst exhibited high levels of a noble metal utilization when used in a PEM fuel cell and had superior durability compared to traditional carbon-based systems [58]. Additionally, we described the influence of the composition of the working atmosphere and the effect of varying the deposition/etching time on the morphology of the modified PEM.

In this paper, we identify another key parameter, the working pressure, used during the sputtering process in the preparation of the modified PEM. This impacted significantly on the resulting morphology and therefore CCM performance. Most importantly however, we demonstrate that the modified membrane is ideal for the anode of a PEM-WE, where it is capable of supporting a thin-film Ir catalyst on its own, therefore completely omitting a corrosion-susceptible catalyst support. This study comprises a morphological characterization of the modified anode-CCM, determination of the electrochemical active surface area (ECSA) via a rotating disk electrode (RDE), and in-cell PEM-WE performance testing, including electrochemical impedance spectroscopy (EIS). We then describe the performance of a modified anode/cathode-CCM, sputter-coated on both sides, i.e. prepared exclusively using dry techniques, yielding remarkable specific current values.

Experimental

Preparation of tested CCMs and corresponding MEAs

Pristine Nafion® NE 1035 membranes (88.9 µm thick, FuelCellStore) were cleaned by blowing the surface with dry nitrogen; they were not cleaned chemically since it is necessary to keep them dry before insertion into a high-vacuum multi-magnetron deposition chamber. The chamber was evacuated to a base pressure of 5.10^{-5} Pa. Mass flow controllers (Alicat) introduced Ar (99.9999%, Linde), and O_2 (99.995%, Linde) gases in a ratio of 65:1. In order to investigate the influence of different working pressures of the Ar:O_2 mixture during the sputter-etching process, four CCMs were prepared. The pressures were set by reducing the pumping speed of a turbomolecular pump to values of 0.2 Pa, 0.4 Pa, 0.6 Pa or 0.8 Pa respectively; pressure was measured using a CMR 365 capacitance gauge (Pfeiffer Vacuum). Subsequently, each of the four membranes was treated similarly with the only exception being the working pressure. By means of a CESAR® RF generator (13.56 MHz) coupled with a NAVIO™ impedance matching device (both from Advanced Energy) the plasma was ignited over the 4″ circular ceramic CeO_2 target (99.99%, K. J. Lesker) and deposition began. The power was set to 65 W, and the deposition time was 70 min, resulting in a layer thickness of 10 nm. Modification of the PEM surface was based on a simultaneous plasma etching and CeO_x deposition during magnetron sputtering. The membrane was etched in places where it was not being protected by the sputtered CeO_x layer that acted as a masking element. In this way, pronounced etched hollows were formed while parts of the membrane that were protected by the CeO_x thin film created fibers. The chamber was then pumped down to base pressure and a working atmosphere of 0.5 Pa was created using Ar alone. By means of a DC01BP power source (K. J. Lesker) the plasma was ignited over the surface of a 2″ circular metallic Ir target (99.9%, K. J. Lesker) and deposition onto the modified surface of the PEM was started. The power was set to 30 W and the deposition time was 30 min, resulting in growth of an Ir thin film with a thickness of 50 nm (i.e. a noble metal loading of 113 µg cm^{-2}). These steps led to the creation of four anode-CCMs, i.e. the catalyst was present only on the modified anode side of the PEM, while the cathode side was intact.

Another two anode-CCMs were prepared to act as references for comparison of our sputter-etching method with more traditional preparations that utilize thin-film deposition. The first reference was a plain PEM with 50 nm of Ir sputtered on its anode side; deposition of the catalyst was carried out the same way as on the four modified PEMs. The second reference was a PEM with 50 nm of Ir sputtered over a 0.2 mg cm^{-2} of TiC-based support sublayer (15 wt% of Nafion® with respect to TiC); again the catalyst was deposited similarly and the preparation details of the TiC-based sublayer are described in our previous work [59]. To complete the MEA, all described anode-CCMs were inserted between a cathode gas

diffusion electrode (GDE) and an anode current collector. The commercial carbon-supported Pt catalyst (Pt 0.5 mg cm^{-2}, FuelCellStore) in the form of a micro porous layer (MPL) on a carbon paper gas diffusion layer (GDL) (Toray) served as a GDE on the cathode side. On the anode side, a porous sintered micro grained titanium GDL (Mott) with a 50 nm protection layer of Pt was used as a current collector.

To demonstrate that our method of PEM modification is convenient for the preparation of a double-sided fully modified membrane, using exclusively dry techniques in a single vacuum entry, i.e. sputter-etched and catalyst-coated from both anode and cathode sides, we prepared the seventh CCM. This last CCM was attached to a special frame-shaped holder that allowed us to sputter-etch both sides of the PEM and consequently deposit 50 nm of Ir on the anode side and 50 nm of Pt on the cathode side. Sputter-etching was performed as described above at a working pressure of 0.4 Pa; Ir deposition was also performed as mentioned previously; Pt deposition was carried out in 0.5 Pa of Ar from a 2″ circular metallic Pt target (99.99%, SAFINA) using the same DC power source as in the case of Ir with power being held at 20 W for 35 min. The MEA was completed by inserting the CCM between a commercial carbon GDL (Sigracet 29 BC) on the cathode side and the previously described titanium GDL on the anode side.

Details of all seven tested MEAs are listed in Table 1.

PEM-WE in-cell performance testing

The performance of each prepared MEA was evaluated in a pneumatically operated single cell (TP-5, Greenlight Innovation) with an active area of 4.62 cm^2. The cathode end plate was made from high-density graphite, the anode end plate from TiN-coated Ti. During the entire operation, cell press pressure was held at 8 bars and the temperature of the cell was kept at 80 °C. A constant flow of 3 ml min^{-1} deionized water (18.2 MΩ cm at 25 °C) was supplied to the anode half-cell. A potentiostat Bio-Logic SP-150 with a 20 A booster was used for the electrochemical analysis.

Before testing the PEM-WE performance, the assembled MEAs within cells underwent a break-in procedure consisting of repetitive switching at 5 min intervals of constant voltage between 1.6 and 1.7 V for a total duration of 3 h, followed by an 8 h long period of 1.7 V constant voltage. Only after this activation were IV curves measured in a fine galvanostatic regime, applying 80 mA steps with a 10 s stabilization period. Electrochemical impedance spectroscopy (EIS) spectra were measured in potentiostatic mode at 1.5 V in the frequency range from 200 kHz to 500 mHz (15 points per decade) with the sine amplitude set to 5 mV. The Nyquist plots of kinetic loops were interpreted considering a simple Randles model [60,61].

RDE samples preparation and testing

Three samples simulating the anode sides of the respective MEAs were prepared to carry out ECSA measurements on an RDE setup; all were deposited on polished glassy carbon (GC) disks. The first sample was a continuous 50 nm thick layer of Ir (resembling the anode of the ***Smooth PEM reference*** MEA). The second sample was a 50 nm thick layer of Ir, sputtered over the 0.2 mg cm^{-2} of TiC-based support sublayer previously dripped on GC (resembling the anode of the ***Ir/TiC reference*** MEA). The third sample was a 50 nm thick layer of Ir, sputtered over the sputter-etched surface of 0.15 mg cm^{-2} of Nafion® previously dripped in the form of a 1 wt% solution onto GC (resembling the anode of the ***0.4 Pa anode-CCM*** MEA). The amount of Nafion® was carefully chosen such that after etching, the GC surface was uncovered in the hollows and after the sputtering of Ir, an electric contact was created between the disk and the catalyst. The sputter-etching process was carried out in a working atmosphere of 0.4 Pa. For all three samples, Ir depositions were performed as described above. Parameters of all three samples for RDE measurements are listed in Table 2.

The RDE setup from Pine Research Instruments with a Pt counter electrode and a Hg/Hg_2SO_4 reference electrode was used for the ECSA evaluation. Individual GC disks with the

Table 1 – List of parameters of seven tested MEAs.

Tested MEAs	Anode side	Cathode side	Ir + Pt loading
0.2 Pa anode-CCM	50 nm Ir (113 μg cm^{-2}) on modified PEM (at 0.2 Pa working pressure) + micro grained Ti GDL (Mott)	GDE (Fuel Cell Store) Pt 500 μg cm^{-2}	613 μg cm^{-2}
0.4 Pa anode-CCM	50 nm Ir (113 μg cm^{-2}) on modified PEM (at 0.4 Pa working pressure) + micro grained Ti GDL (Mott)	GDE (Fuel Cell Store) Pt 500 μg cm^{-2}	613 μg cm^{-2}
0.6 Pa anode-CCM	50 nm Ir (113 μg cm^{-2}) on modified PEM (at 0.6 Pa working pressure) + micro grained Ti GDL (Mott)	GDE (Fuel Cell Store) Pt 500 μg cm^{-2}	613 μg cm^{-2}
0.8 Pa anode-CCM	50 nm Ir (113 μg cm^{-2}) on modified PEM (at 0.8 Pa working pressure) + micro grained Ti GDL (Mott)	GDE (Fuel Cell Store) Pt 500 μg cm^{-2}	613 μg cm^{-2}
Smooth PEM reference	50 nm Ir (113 μg cm^{-2}) on smooth PEM + micro grained Ti GDL (Mott)	GDE (Fuel Cell Store) Pt 500 μg cm^{-2}	613 μg cm^{-2}
Ir/TiC reference	50 nm Ir (113 μg cm^{-2}) on TiC-based sublayer + micro grained Ti GDL (Mott)	GDE (Fuel Cell Store) Pt 500 μg cm^{-2}	613 μg cm^{-2}
0.4 Pa anode/cathode-CCM	50 nm Ir (113 μg cm^{-2}) on modified PEM (at 0.4 Pa working pressure) + micro grained Ti GDL (Mott)	50 nm Pt (107 μg cm^{-2}) on modified PEM (at 0.4 Pa working pressure) + GDL (Sigracet 29 BC, Fuel Cell Store)	220 μg cm^{-2}

layers to be investigated were used as the working electrodes. The 0.1 M H_2SO_4 electrolyte was purged with N_2 for 1 h prior to the measurements as well as throughout the experiment. The rotating speed was set to 2500 rpm. Using a Bio-Logic SP-50 potentiostat, each sample was cycled in the narrow interval from 0.0 V to 0.6 V versus RHE in order to avoid Ir oxidation, which would prevent hydrogen from being adsorbed onto the surface of the catalyst. The ECSA was determined by integrating the H_{UPD} region and using 179 μC cm_{Ir}^{-2} constant for the charge value per surface unit [62].

Morphological analysis

The top view morphologies of CCMs were probed by scanning electron microscopy (SEM), using a Tescan MIRA 3 apparatus, operating at an accelerating voltage of 10 kV. Cross-sectional views of CCMs were obtained by transmission electron microscopy (TEM) using a 200 kV JEOL JEM NEOARM-200F microscope. The samples for TEM observations in the form of very thin lamellas, were prepared by the lift-off technique, utilizing a gallium focused ion beam (FIB) of a Tescan LYRA dual beam microscope. A silicon oxide layer prepared by electron beam-induced and subsequent ion beam-induced deposition was applied to protect the membrane during the lift-off process.

Results and discussion

Effect of working pressure on the morphologies of modified membranes during sputter-etching and its impact on MEA performance in a PEM-WE cell

Even though the process of simultaneous etching of the PEM and sputtering the material onto its surface is very straightforward, facilitating the creation of a large surface area for catalyst dispersal without the need for additional nanoparticles, and using a combination of dry and wet techniques, the process still has to be carried out using utmost precision in order to obtain the desired morphology. The etching agent, i.e. oxygen and inert sputter gas (argon) must be mixed in the correct ratio and the DC power and duration of the process has to be chosen accordingly [58]. The working pressure also needs to be precisely controlled during the sputtering process. Fig. 2 shows different morphologies of four anode-CCMs that were deposited similarly with the exception of the working pressure, which ranged from 0.2 Pa to 0.8 Pa (additional high-resolution TEM images can be found in Ref. [58]). Corresponding in-cell PEM-WE performances, i.e. IV curves of assembled MEAs with individual anode-CCMs are plotted in Fig. 3.

Based on the top-view SEM images (Fig. 2, top row), it can be concluded that lowering the working pressure resulted in a more pronounced porous structure. TEM cross-sectional images (Fig. 2, middle row) further confirmed this and allowed us to determinate the actual length of individual fibers. In addition, the material contrast between ionomer and subsequently deposited Ir catalyst (Fig. 2, bottom row) enabled us to estimate its dispersion over the fiber structure. Clearly, a denser field of shorter fibers (i.e. structures sputter-etched at 0.6 Pa and 0.8 Pa) tended to be covered predominantly from the top, resulting in a nearly continuous layer at the surface, while the larger spacing between longer fibers (i.e. structures sputter-etched at 0.2 Pa and 0.4 Pa) favored a more even catalyst distribution over the surface. Based on these observations, a working pressure of 0.2 Pa would seem to be an ideal value for the sputter-etching procedure. Note however that decreasing the working pressure below 0.2 Pa is not possible since the glow discharge on the magnetron head ceases to be stable.

When comparing actual in-cell performances, we noted that the ***0.2 Pa anode-CCM*** was not the most efficiently performing MEA, but the ***0.4 Pa anode-CCM*** was. A current density of 3180 mA cm^{-2} at 1.9 V was achieved, surpassing the ***0.6 Pa anode-CCM*** by 200 mA cm^{-2}, the ***0.2 Pa anode-CCM*** by 720 mA cm^{-2} and the ***0.8 Pa anode-CCM*** by 950 mA cm^{-2}. Increasing the PEM porosity with a fixed thin-film catalyst loading did not automatically translate into higher performance, which seemed counter-intuitive. However, taking our previous results into account [58] and looking again at the TEM cross-sections we determined that dispersion of a given amount of metal over a significantly enlarged surface inevitably led to disruptions of electron pathways; i.e. lateral conductivity was insufficient, some regions of the PEM were therefore inactive and performance was inferior. On the other hand, when the sputter-etching process was carried out at higher pressures, the fibers were shorter and denser. The catalyst was thus deposited mostly on the tips of fibers rather than on the body, resulting in poor dispersion and again worsened performance.

Therefore, based on the in-cell comparison of tested CCMs shown in Fig. 3, we show that 0.4 Pa is the ideal working pressure that results in an optimal morphology and, in combination with 50 nm of subsequently sputtered Ir catalyst, yields maximal PEM-WE performance. The ***0.4 Pa anode-CCM*** was used therefore in the following comparative investigation.

Comparison of MEA with sputter-etched anode-CCM and conventionally prepared MEAs

In the former section, we have identified the optimal sputtering pressure for the preparation of the anode-CCM, which,

Table 2 – List of parameters of three tested RDE samples.

Tested samples	Rotating disk electrode	Catalytic layer
Smooth RDE	Glassy carbon	50 nm Ir (113 μg cm^{-2})
TiC RDE	Glassy carbon	0.2 mg cm^{-2} of TiC sublayer + 50 nm Ir (113 μg cm^{-2})
Sputter-etched RDE	Glassy carbon	0.15 mg cm^{-2} of sputter-etched Nafion® at 0.4 Pa + 50 nm Ir (113 μg cm^{-2})

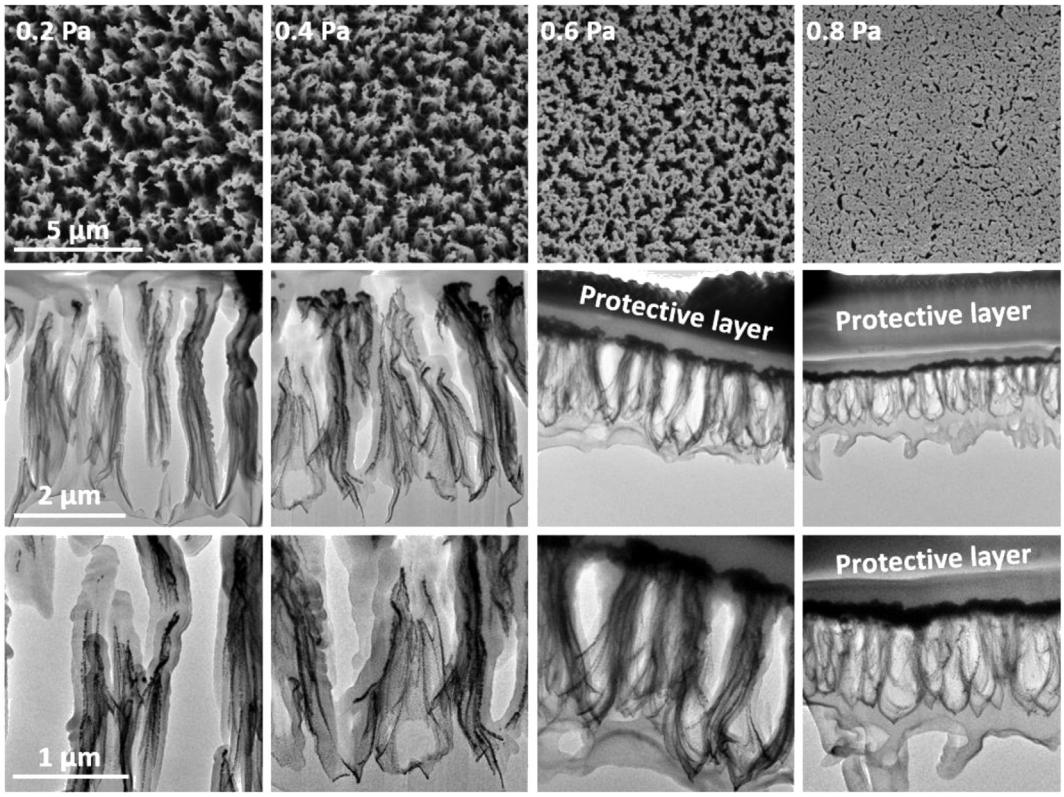

Fig. 2 – Top-view SEM micrographs of sputter-etched structures formed at different working pressures (top row) and corresponding cross-sectional TEM views (middle and bottom rows); sets of SEM and TEM images in respective rows are taken with the same magnification.

in conjunction with other previously studied and tuned up parameters, leads to maximal PEM-WE in-cell efficiency. We then compared the best performing MEA using the optimized anode-CCM (i.e. ***0.4 Pa anode-CCM***) with other MEAs containing more conventional anode-CCMs; namely, to an MEA with plain untreated PEM, sputtered over with Ir on its anode side (i.e. ***Smooth PEM reference***) and an MEA with TiC-supported Ir sputtered on its anode side (i.e. ***Ir/TiC reference***; this system was developed and discussed in Ref. [59,63]). Fig. 4 Shows the morphology of these anode-CCMs. Fig. 5a comprises IV curves of MEAs with the same noble metal loading within the PEM-WE cell, Fig. 5b compares their EIS characteristics.

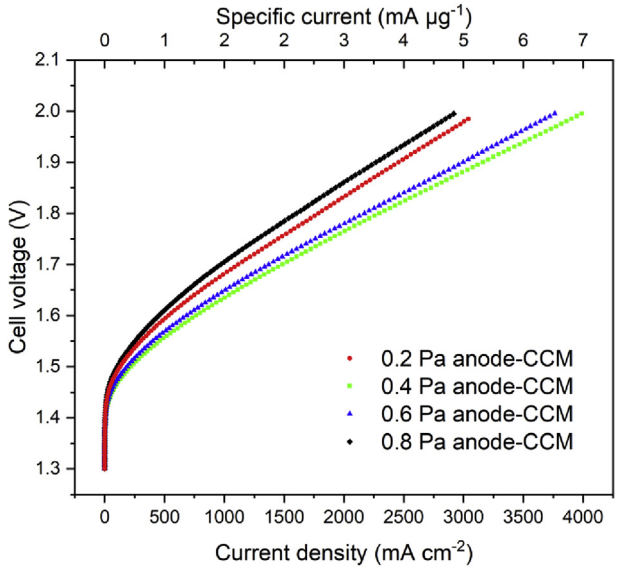

Fig. 3 – PEM-WE IV curves of MEAs with anode-CCMs, sputter-etched at different working pressures.

As expected, due to the low specific area of the flat membrane surface, the ***Smooth PEM reference*** performed far worse than both MEAs with enlarged surfaces on the anode side. A difference between the ***Ir/TiC reference*** and the ***0.4 Pa anode-CCM*** was also noticeable, the sputter-etched anode surpassed the TiC-based system by 370 mA cm^{-2} at 1.9 V. In addition, from a practical point of view, the completely dry preparation process of the ***0.4 Pa anode-CCM*** was significantly less complex and less prone to error than that of the ***Ir/TiC reference,*** which consisted of a multistage combination of wet and dry techniques and hot-press support transitions [59].

Another key aspect is that the sputter-etching process did not increase the overall ohmic losses of the MEA. The EIS spectra in Fig. 5b, show that the ***0.4 Pa anode-CCM*** not only featured a smaller semi-arc in the negative imaginary half-plane, i.e. improved reaction kinetics [64] in contrast to other MEAs, but it also had practically the same ohmic resistance (the high frequency intercept on the X-axis) as the

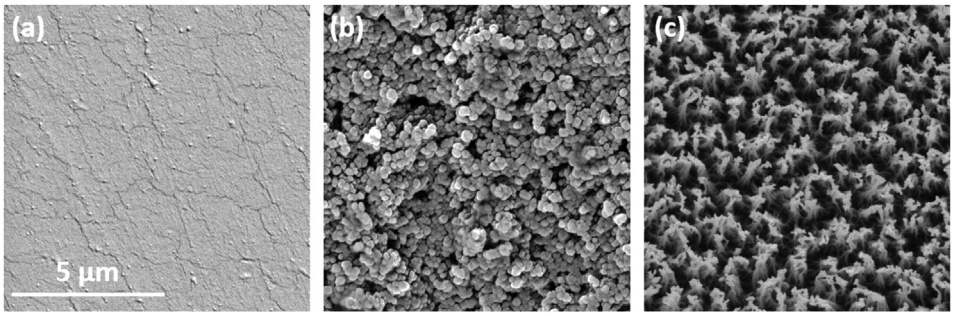

Fig. 4 – Top-view SEM micrographs of *Smooth PEM reference* (a), *Ir/TiC reference* (b) and *0.4 Pa anode-CCM* (c); images are taken at the same magnification.

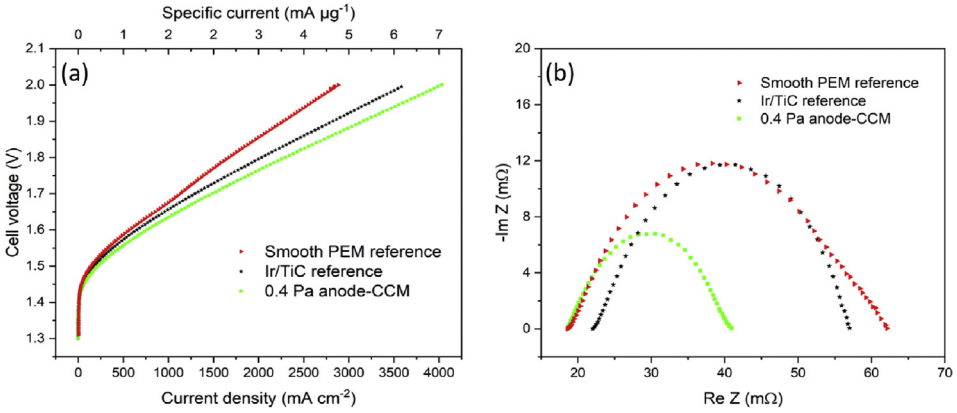

Fig. 5 – PEM-WE IV curves (a) and Nyquist plots (b) of *Smooth PEM reference*, *Ir/TiC reference* and *0.4 Pa anode-CCM*.

Smooth PEM reference. This was not true for the *Ir/TiC reference*, which here represents a design relying on an additional nanoparticle-based support layer being present on the actual PEM for catalyst dispersion. Low ohmic resistance is a particularly important parameter should the system operate at very high current densities, since it can have a much larger impact on the cell voltage than the actual improvement in kinetics [65]. Also, the fact that improved *0.4 Pa anode-CCM* performance stems from the morphological alteration of the PEM surface is convenient from an industrial standpoint since the modification process is catalyst-independent and therefore, is fully compatible with any other novel thin-film catalyst that might, in the future, replace iridium.

To further demonstrate that the enhanced *0.4 Pa anode-CCM* performance was an effect of a larger surface, we conducted an ECSA assessment using the RDE setup. Three samples simulating the anode-CCM of respective MEAs, the *Smooth RDE*, *TiC RDE* and *sputter-etched RDE* (details are given in Table 2) were tested. Cyclic voltammograms are plotted in Fig. 6.

In contrast to the *Smooth RDE* and the *Sputter-etched RDE* samples, the CV of the *TiC RDE* exhibited a much higher double-layer capacitance, reflecting a considerable increment in the interfacial capacitance due to the presence of 0.2 mg cm^{-2} of TiC-based sublayer between the GC electrode surface and the 50 nm Ir thin film. The ECSA values, obtained

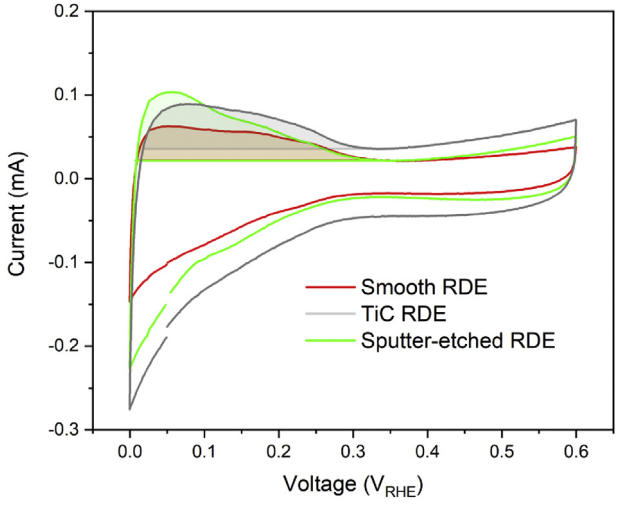

Fig. 6 – Cyclic voltammograms obtained from *Smooth RDE*, *TiC RDE* and *Sputter-etched RDE* samples with integrated H_{UPD} regions.

Table 3 – Integrated charges and corresponding ECSA values obtained from cyclic voltammograms presented in Fig. 6

Sample	Integrated charge [µC]	ECSA [cm^2 mg^{-1}]
Smooth RDE	118.9	30
TiC RDE	218.6	55
Sputter-etched RDE	276.2	70

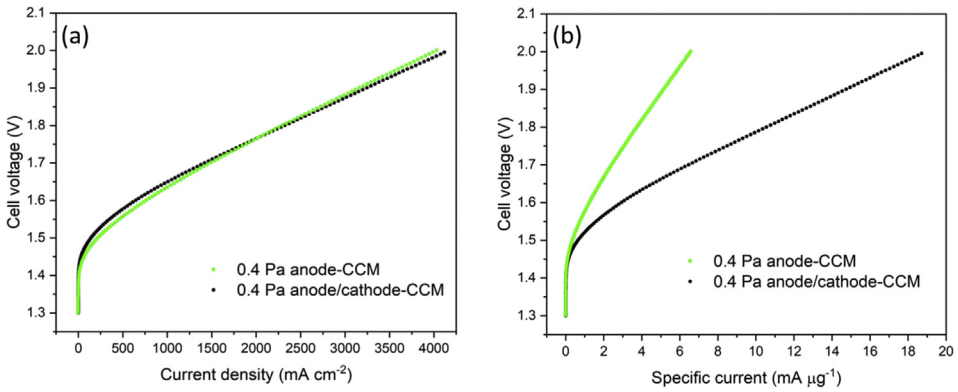

Fig. 7 – PEM-WE IV curves in absolute current density (a) and specific current density (b) of the *0.4 Pa anode-CCM* and the *0.4 Pa anode/cathode-CCM*.

by integration of the H_{UPD} region (see Table 3), confirmed that the ***Sputter-etched RDE*** indeed had the largest surface, nearly 30% and 130% larger than the ***TiC RDE*** and the ***Smooth RDE*** samples, respectively.

It should be emphasized that the actual increment in ECSA of the sputter-etched ***0.4 Pa anode-CCM*** compared with the ***Smooth PEM reference*** and the ***Ir/TiC reference*** samples is most likely larger than indicated by the RDE experiment. The reason is that the Nafion® layer on GC had to be relatively thin in order to secure electrical contact after the sputter-etching process and subsequent Ir coating, as such formed fibers were not as long as in case of the ***0.4 Pa anode-CCM***. Nonetheless, this measurement proves that the increased efficiency of the sputter-etched CCM was indeed related to its increased ECSA.

Performance of the MEA with the CCM prepared exclusively by means of the dry technique

The results above show that the sputter-etched and subsequently Ir-coated PEM performed remarkably well as the anode-CCM in PEM-WE. A question arises whether it is also possible to employ the sputter-etching process on the cathode side of PEM, i.e. creating a full anode/cathode-CCM prepared exclusively using dry techniques that would retain the efficiency of higher loading systems. We tested therefore the performance of the all dry ***0.4 Pa anode/cathode-CCM*** and compared it with the ***0.4 Pa anode-CCM*** with a commercial cathode, the difference between the two being the cathode composition and Pt loading (see Table 1). Fig. 7a shows that despite having a significantly lower combined Pt + Ir metal loading (220 μg cm^{-2} vs. 613 μg cm^{-2}) the all dry ***0.4 Pa anode/cathode-CCM*** performed surprisingly well, similar to the ***0.4 Pa anode-CCM*** with a commercial cathode.

Although the latter ran slightly more efficiently in the activation-polarisation part of the IV curve, which is mostly influenced by the amount of catalyst itself, the concentration-polarisation part at high current densities favored the ***0.4 Pa anode/cathode-CCM*** [66]. This phenomenon is presumably connected with the absence, or better said replacement of the relatively thick MPL of carbon black, ionomer and Pt catalyst with the more streamlined sputter-etched structure of the Pt-coated PEM.

Moreover, it is interesting to compare the two tested CCMs in terms of specific current, i.e. current density normalized to noble metal loading (see Fig. 7b). The all dry ***0.4 Pa anode/cathode-CCM*** exhibited a more than three times higher specific current at 1.9 V than the ***0.4 Pa anode-CCM***, containing a commercial cathode. This further emphasizes the application potential of sputter-etched PEMs, as catalyst reduction is one of the top priorities in regard to the commercialization of PEM-WE technology.

Conclusions

In this study, it was demonstrated that a highly porous fiber-like structure on the surface of the PEM, formed by concurrent plasma etching and material deposition during reactive magnetron sputtering of CeO_x, can act as an efficient support for thin-film anode catalysts to be used in PEM-WE applications. The undisputable advantage of this approach is that it allows the complete omission of nanoparticle-based support material for catalyst dispersion, which is often prone to corrosion due to high operational potentials during the OER.

It was shown that aside from other previously studied parameters, the working pressure during the sputter-etching process plays a crucial role in tuning the porosity and morphology of the resultant structure. The lower the pressure, the more pronounced the porous surface and the longer the individual fibers; however, this does not necessarily lead to better PEM-WE performance because the sputter-etched structure must be covered continuously by a thin-film catalyst to ensure proper electron conductivity. The preset thickness (50 nm) of sputtered catalyst, covering a moderately sputter-etched surface that was formed at an increased working pressure, yielded the highest current density.

The CCM with the sputter-etched anode side outperformed the CCM with the plain PEM surface as well as the CCM with the TiC-based support sublayer. EIS analysis revealed that sputter-etching leads to faster reaction kinetics, yet it did not

increase the overall ohmic resistance of the CCM - it remained unchanged with respect to CCM with the plain PEM, unlike in case of the CCM with a TiC-based sublayer.

RDE measurements confirmed ECSA enhancement of the sputter-etched PEM by approximately 30% compared to the PEM covered by the TiC-based support sublayer, and by 130% with respect to the plain PEM surface.

The sputter-etching process was then employed to modify the surface of a PEM from both sides. It was shown that using a frame-shaped holder and a multi-magnetron setup it was possible to carry out the modification and subsequent catalyst deposition in a single vacuum entry. As a result, a remarkably performing CCM with a thin-film anode and cathode catalyst, supported on the sputter-etched surface of a PEM was prepared, solely using a dry vacuum coating technique – magnetron sputtering. The use of a single industrially widespread method has therefore the potential to simplify and accelerate the manufacturing process in the context of large-scale production. In addition, should the future bring more active catalysts than Ir and Pt, conveniently the sputter-etched PEM will be fully compatible with any novel material deposited in the form of a thin film.

Acknowledgement

This work was supported financially by the Czech Science Foundation (grant No. 18-06989Y), Grant Agency of the Charles University in Prague (GAUK No. 58620) and the structural funds project No. CZ.02.1.01/0.0/0.0/16_025/0007414. We would like to acknowledge the OP VVV "Excellent Research Teams", project No. CZ.02.1.01/0.0/0.0/15_003/0000417 – CUCAM for the electron microscopy. J.N. is grateful for the financial support of the Martina Roeselová Foundation. Furthermore, the authors acknowledge the CERIC-ERIC consortium for access to experimental facilities. Lastly, T.H. and P.K. would like to thank Dr. Maryna Vorokhta for valuable discussions.

REFERENCES

[1] Kousksou T, Bruel P, Jamil A, El Rhafiki T, Zeraouli Y. Energy storage: applications and challenges. Sol Energy Mater Sol Cells 2014;120:59–80. https://doi.org/10.1016/j.solmat.2013.08.015.

[2] Zakeri B, Syri S. Electrical energy storage systems: a comparative life cycle cost analysis. Renew Sustain Energy Rev 2015;42:569–96. https://doi.org/10.1016/j.rser.2014.10.011.

[3] Luo X, Wang J, Dooner M, Clarke J. Overview of current development in electrical energy storage technologies and the application potential in power system operation q. Appl Energy 2015;137:511–36. https://doi.org/10.1016/j.apenergy.2014.09.081.

[4] Aneke M, Wang M. Energy storage technologies and real life applications – a state of the art review. Appl Energy 2016;179:350–77. https://doi.org/10.1016/j.apenergy.2016.06.097.

[5] Abe JO, Popoola API, Ajenifuja E, Popoola OM. Hydrogen energy, economy and storage: review and recommendation. Int J Hydrogen Energy 2019;44:15072–86. https://doi.org/10.1016/j.ijhydene.2019.04.068.

[6] Armaroli N, Balzani V. The hydrogen issue. ChemSusChem 2011;4:21–36. https://doi.org/10.1002/cssc.201000182.

[7] Winter C-J. Hydrogen energy — abundant, efficient, clean: a debate over the energy-system-of-change☆. Int J Hydrogen Energy 2009;34:S1–52. https://doi.org/10.1016/j.ijhydene.2009.05.063.

[8] Mazloomi K, Gomes C. Hydrogen as an energy carrier: prospects and challenges. Renew Sustain Energy Rev 2012;16:3024–33. https://doi.org/10.1016/j.rser.2012.02.028.

[9] Ursua A, Gandia LMLM, Sanchis P. Hydrogen production from water electrolysis: current status and future trends. Proc IEEE 2012;100:410–26. https://doi.org/10.1109/JPROC.2011.2156750.

[10] Buttler A, Spliethо H. Current status of water electrolysis for energy storage, grid balancing and sector coupling via power-to-gas and power-to-liquids. Rev 2018;82:2440–54. https://doi.org/10.1016/j.rser.2017.09.003.

[11] Carmo M, Fritz DL, Mergel J, Stolten D. A comprehensive review on PEM water electrolysis. Int J Hydrogen Energy 2013;38:4901–34. https://doi.org/10.1016/j.ijhydene.2013.01.151.

[12] Schmidt O, Gambhir A, Staffell I, Hawkes A, Nelson J, Few S. Future cost and performance of water electrolysis: an expert elicitation study. Int J Hydrogen Energy 2017;42:30470–92. https://doi.org/10.1016/j.ijhydene.2017.10.045.

[13] Katsounaros I, Cherevko S, Zeradjanin AR, Mayrhofer KJJ. Oxygen electrochemistry as a cornerstone for sustainable energy conversion. Angew Chem Int Ed 2014;53:102–21. https://doi.org/10.1002/anie.201306588.

[14] Fabbri E, Schmidt TJ. Oxygen evolution reaction—the enigma in water electrolysis. ACS Catal 2018;8:9765–74. https://doi.org/10.1021/acscatal.8b02712.

[15] Lasia A. Mechanism and kinetics of the hydrogen evolution reaction. Int J Hydrogen Energy 2019;44:19484–518. https://doi.org/10.1016/j.ijhydene.2019.05.183.

[16] Eftekhari A. Electrocatalysts for hydrogen evolution reaction. Int J Hydrogen Energy 2017;42:11053–77. https://doi.org/10.1016/j.ijhydene.2017.02.125.

[17] Kim JS, Kim B, Kim H, Kang K. Recent progress on multimetal oxide catalysts for the oxygen evolution reaction. Adv Energy Mater 2018;8:1702774. https://doi.org/10.1002/aenm.201702774.

[18] Fabbri E, Habereder A, Waltar K, Kötz R, Schmidt TJ. Developments and perspectives of oxide-based catalysts for the oxygen evolution reaction. Catal Sci Technol 2014;4:3800–21. https://doi.org/10.1039/C4CY00669K.

[19] Antolini E. Iridium as catalyst and cocatalyst for oxygen evolution/reduction in acidic polymer electrolyte membrane electrolyzers and fuel cells. ACS Catal 2014;4:1426–40. https://doi.org/10.1021/cs4011875.

[20] Li X, Hao X, Abudula A, Guan G. Nanostructured catalysts for electrochemical water splitting: current state and prospects. J Mater Chem 2016;4:11973–2000. https://doi.org/10.1039/C6TA02334G.

[21] Ma Z, Zhang Y, Liu S, Xu W, Wu L, Hsieh Y-C, et al. Reaction mechanism for oxygen evolution on RuO_2, IrO_2, and RuO_2@IrO_2 core-shell nanocatalysts. J Electroanal Chem 2018;819:296–305. https://doi.org/10.1016/j.jelechem.2017.10.062.

[22] Nong HN, Gan L, Willinger E, Teschner D, Strasser P. IrO_x core-shell nanocatalysts for cost- and energy-efficient electrochemical water splitting. Chem Sci 2014;5:2955–63. https://doi.org/10.1039/C4SC01065E.

[23] Nong HN, Oh H-S, Reier T, Willinger E, Willinger M-G, Petkov V, et al. Oxide-supported $IrNiO_x$ core-shell particles as efficient, cost-effective, and stable catalysts for

electrochemical water splitting. Angew Chem Int Ed 2015;54:2975–9. https://doi.org/10.1002/anie.201411072.
[24] Antolini E, Gonzalez ER. Carbon supports for low-temperature fuel cell catalysts. Appl Catal B Environ 2009;88:1–24. https://doi.org/10.1016/j.apcatb.2008.09.030.
[25] Wang Y, Chen KS, Mishler J, Cho SC, Adroher XC. A review of polymer electrolyte membrane fuel cells: technology, applications, and needs on fundamental research. Appl Energy 2011;88:981–1007. https://doi.org/10.1016/j.apenergy.2010.09.030.
[26] Bard AJ, Parsons R, Jordan J. International union of pure and applied chemistry. Standard potentials in aqueous solution. 1985.
[27] Kinoshita K. Carbon: electrochemical and physicochemical properties. Wiley; 1988.
[28] Mazúr P, Polonský J, Paidar M, Bouzek K. Non-conductive TiO_2 as the anode catalyst support for PEM water electrolysis. Int J Hydrogen Energy 2012;37:12081–8. https://doi.org/10.1016/j.ijhydene.2012.05.129.
[29] Xu J, Liu G, Li J, Wang X. The electrocatalytic properties of an IrO_2/SnO_2 catalyst using SnO_2 as a support and an assisting reagent for the oxygen evolution reaction. Electrochim Acta 2012;59:105–12. https://doi.org/10.1016/j.electacta.2011.10.044.
[30] Slavcheva E, Borisov G, Lefterova E, Petkucheva E, Boshnakova I. Ebonex supported iridium as anode catalyst for PEM water electrolysis. Int J Hydrogen Energy 2015;40:11356–61. https://doi.org/10.1016/j.ijhydene.2015.03.005.
[31] Karimi F, Peppley BA. Metal carbide and oxide supports for iridium-based oxygen evolution reaction electrocatalysts for polymer-electrolyte-membrane water electrolysis. Electrochim Acta 2017;246:654–70. https://doi.org/10.1016/j.electacta.2017.06.048.
[32] Bele M, Stojanovski K, Jovanovič P, Moriau L, Koderman Podboršek G, Moškon J, et al. Towards stable and conductive titanium oxynitride high-surface-area support for iridium nanoparticles as oxygen evolution reaction electrocatalyst. ChemCatChem 2019;11:5038–44. https://doi.org/10.1002/cctc.201901487.
[33] Polonský J, Mazúr P, Paidar M, Christensen E, Bouzek K. Performance of a PEM water electrolyser using a TaC-supported iridium oxide electrocatalyst. Int J Hydrogen Energy 2014;39:3072–8. https://doi.org/10.1016/j.ijhydene.2013.12.085.
[34] Puthiyapura VK, Pasupathi S, Su H, Liu X, Pollet B, Scott K. Investigation of supported IrO_2 as electrocatalyst for the oxygen evolution reaction in proton exchange membrane water electrolyser. Int J Hydrogen Energy 2014;39:1905–13. https://doi.org/10.1016/j.ijhydene.2013.11.056.
[35] Ma L, Sui S, Zhai Y. Preparation and characterization of Ir/TiC catalyst for oxygen evolution. J Power Sources 2008;177:470–7. https://doi.org/10.1016/j.jpowsour.2007.11.106.
[36] Nikiforov AV, Petrushina IM, Prag CB, Polonsky J, Christensen E, Bjerrum NJ. Development and study of tantalum and niobium carbides as electrocatalyst supports for the oxygen electrode for PEM water electrolysis at elevated temperatures. ECS Trans 2013;45:59–67. https://doi.org/10.1149/04521.0059ecst.
[37] Ma L, Sui S, Zhai Y. Investigations on high performance proton exchange membrane water electrolyzer. Int J Hydrogen Energy 2009;34:678–84. https://doi.org/10.1016/j.ijhydene.2008.11.022.
[38] Haviar S, Dubau M, Lavková J, Khalakhan I, Potin V, Matolín V, et al. Investigation of growth mechanism of thin sputtered cerium oxide films on carbon substrates. Sci Adv Mater 2014;6:1278–85. https://doi.org/10.1166/sam.2014.1905.
[39] Dubau M, Lavková J, Khalakhan I, Haviar S, Potin V, Matolín V, et al. Preparation of magnetron sputtered thin cerium oxide films with a large surface on silicon substrates using carbonaceous interlayers. ACS Appl Mater Interfaces 2014;6:1213–8. https://doi.org/10.1021/am4049546.
[40] Khalakhan I, Dubau M, Haviar S, Lavková J, Matolínová I, Potin V, et al. Growth of nano-porous Pt-doped cerium oxide thin films on glassy carbon substrate. Ceram Int 2013;39:3765–9. https://doi.org/10.1016/j.ceramint.2012.10.215.
[41] Lavkova J, Khalakhan I, Chundak M, Vorokhta M, Potin V, Matolin V, et al. Growth and composition of nanostructured and nanoporous cerium oxide thin films on a graphite foil. Nanoscale 2015;7:4038–47. https://doi.org/10.1039/c4nr06550f.
[42] Nováková J, Dubau M, Š Fuka, Duchoň T, Johánek V, Fiala R, et al. Role of nitrogenated carbon in tuning Pt-CeO_x based anode catalysts for higher performance of hydrogen-powered fuel cells. Appl Surf Sci 2020;515:146054. https://doi.org/10.1016/j.apsusc.2020.146054.
[43] Vorokhta M, Khalakhan I, Václavů M, Kovács G, Kozlov SMSM, Kúš P, et al. Surface composition of magnetron sputtered Pt-Co thin film catalyst for proton exchange membrane fuel cells. Appl Surf Sci 2016;365:245–51. https://doi.org/10.1016/j.apsusc.2016.01.004.
[44] Ostroverkh A, Johanek V, Dubau M, Kus P, Veltruska K, Vaclavu M, et al. Novel fuel cell MEA based on Pt-C deposited by magnetron sputtering. ECS Trans 2017;80. https://doi.org/10.1149/08008.0225ecst.
[45] Khalakhan I, Fiala R, Lavková J, Kúš P, Ostroverkh A, Václavů M, et al. Candle soot as efficient support for proton exchange membrane fuel cell catalyst. Fuel Cell 2016;16:652–5. https://doi.org/10.1002/fuce.201600016.
[46] Ostroverkh A, Dubau M, Khalakhan I, Fiala R, Ostroverkh Y, Science P. Optimization of ionomer-free Pt catalyst for anode/cathode of PEMFC via magnetron sputtering. 2018.
[47] Fiala R, Vaclavu M, Rednyk A, Khalakhan I, Vorokhta M, Lavkova J, et al. Pt–CeO_x thin film catalysts for PEMFC. Catal Today 2015;240:236–41. https://doi.org/10.1016/j.cattod.2014.03.069.
[48] Labou D, Slavcheva E, Schnakenberg U, Neophytides S. Performance of laboratory polymer electrolyte membrane hydrogen generator with sputtered iridium oxide anode. J Power Sources 2008;185:1073–8. https://doi.org/10.1016/j.jpowsour.2008.08.013.
[49] Slavcheva E, Radev I, Bliznakov S, Topalov G, Andreev P, Budevski E. Sputtered iridium oxide films as electrocatalysts for water splitting via PEM electrolysis. Electrochim Acta 2007;52:3889–94. https://doi.org/10.1016/j.electacta.2006.11.005.
[50] Sapountzi FM, Divane SC, Papaioannou EI, Souentie S, Vayenas CG. The role of Nafion content in sputtered IrO_2 based anodes for low temperature PEM water electrolysis. J Electroanal Chem 2011;662:116–22. https://doi.org/10.1016/j.jelechem.2011.04.005.
[51] Ostroverkh A, Dubau M, Kúš P, Haviar S, Václavů M, Šmíd B, et al. Durable ultra-low-platinum ionomer-free anode catalyst for hydrogen proton exchange membrane fuel cell. Int J Energy Res 2020;44:4641–51. https://doi.org/10.1002/er.5245.
[52] Omosebi A, Besser RS. Ultra-low mass sputtered and conventional catalyst layers on plasma- etched nafion for PEMFC applications. 2017. p. 762–9. https://doi.org/10.1002/fuce.201600183.
[53] Debe MK. Tutorial on the fundamental characteristics and practical properties of nanostructured thin film. NSTF)

Catalysts 2013;160:522–34. https://doi.org/10.1149/2.049306jes.
[54] Liu G, Xu J, Wang Y, Wang X. An oxygen evolution catalyst on an antimony doped tin oxide nanowire structured support for proton exchange membrane liquid water electrolysis. J Mater Chem 2015;3:20791–800. https://doi.org/10.1039/C5TA02942B.
[55] Ye F, Hu W, Liu H, Liu J, Li J, Wang X, et al. Pt-IrO_2 nanorod array electrode for oxygen evolution in PEM water electrolysis cell. Asia Pac J Chem Eng 2013;8:271–7. https://doi.org/10.1002/apj.1675.
[56] Weber D, Schoop LM, Wurmbrand D, Laha S, Podjaski F, Duppel V, et al. IrOOH nanosheets as acid stable electrocatalysts for the oxygen evolution reaction. J Mater Chem 2018;6:21558–66. https://doi.org/10.1039/C8TA07950A.
[57] Shi Q, Zhu C, Du D, Wang J, Xia H, Engelhard MH, et al. Ultrathin dendritic IrTe nanotubes for an efficient oxygen evolution reaction in a wide pH range. J Mater Chem 2018;6:8855–9. https://doi.org/10.1039/C8TA01288A.
[58] Yakovlev YV, Nováková J, Kúš P, Dinhová TN, Matolínová I, Matolín V. Highly developed nanostructuring of polymer-electrolyte membrane supported catalysts for hydrogen fuel cell application. J Power Sources 2019;439:227084. https://doi.org/10.1016/j.jpowsour.2019.227084.
[59] Kúš P, Ostroverkh A, Ševčíková K, Khalakhan I, Fiala R, Skála T, et al. Magnetron sputtered Ir thin film on TiC-based support sublayer as low-loading anode catalyst for proton exchange membrane water electrolysis. Int J Hydrogen Energy 2016;41:15124–32. https://doi.org/10.1016/j.ijhydene.2016.06.248.
[60] Yuan X, Wang H, Colin Sun J, Zhang J. AC impedance technique in PEM fuel cell diagnosis-A review. Int J Hydrogen Energy 2007;32:4365–80. https://doi.org/10.1016/j.ijhydene.2007.05.036.
[61] Brunetto C, Moschetto A, Tina G. PEM fuel cell testing by electrochemical impedance spectroscopy. Elec Power Syst Res 2009;79:17–26. https://doi.org/10.1016/j.epsr.2008.05.012.
[62] Alia SM, Hurst KE, Kocha SS, Pivovar BS. Mercury underpotential deposition to determine iridium and iridium oxide electrochemical surface areas. J Electrochem Soc 2016;163:F3051–6. https://doi.org/10.1149/2.0071611jes.
[63] Kúš P, Ostroverkh A, Khalakhan I, Fiala R, Kosto Y, Šmíd B, et al. Magnetron sputtered thin-film vertically segmented Pt-Ir catalyst supported on TiC for anode side of proton exchange membrane unitized regenerative fuel cells. Int J Hydrogen Energy 2019;44:16087–98. https://doi.org/10.1016/j.ijhydene.2019.04.216.
[64] Hu J. Oxygen evolution reaction on IrO_2-based DSA® type electrodes: kinetics analysis of Tafel lines and EIS. Int J Hydrogen Energy 2004;29:791–7. https://doi.org/10.1016/j.ijhydene.2003.09.007.
[65] Debe MK. Electrocatalyst approaches and challenges for automotive fuel cells. Nature 2012;486:43–51. https://doi.org/10.1038/nature11115.
[66] van der Merwe J, Uren K, van Schoor G, Bessarabov D. Characterisation tools development for PEM electrolysers. Int J Hydrogen Energy 2014;39:14212–21. https://doi.org/10.1016/j.ijhydene.2014.02.096.